

# Sedimentation dynamics in the East China Sea elucidated from $^{210}\text{Pb}$ , $^{137}\text{Cs}$ and $^{239,240}\text{Pu}$

Chih-An Huh <sup>a,\*</sup>, Chih-Chieh Su <sup>a,b</sup>

<sup>a</sup> Institute of Earth Sciences, Academia Sinica, P.O. Box 1-55, Nankang, Taipei, Taiwan

<sup>b</sup> Institute of Oceanography, National Taiwan University, Taipei, Taiwan

Received 2 September 1998; accepted 4 March 1999

## Abstract

Sedimentation dynamics in the East China Sea was investigated based on profiles and inventories of  $^{210}\text{Pb}_{\text{ex}}$ ,  $^{137}\text{Cs}$  and  $^{239,240}\text{Pu}$  in sediment cores collected from various settings in this marginal sea. The derived sedimentation rates vary by two orders of magnitude, from  $\sim 2$  to  $0.02 \text{ cm yr}^{-1}$ , and generally decrease southward along the inner shelf and eastward offshore. This pattern is consistent with the dispersal of Yangtze River-derived sediments by the current and tidal systems. The weighted mean sedimentation rate over the shelf (ca.  $0.3 \text{ g cm}^{-2} \text{ yr}^{-1}$ ) appears to be higher than fluvial inputs from the Yangtze River and Taiwan ( $0.14 \text{ g cm}^{-2} \text{ yr}^{-1}$ ). The discrepancy can be reduced by considering the effect of sediment mixing (which renders sedimentation rates overestimated) and the possibility of additional sediment input from the Yellow River's dispersal system. Spatial variations of the observed nuclide inventories in sediments suggest extensive sediment redistribution, boundary scavenging of  $^{210}\text{Pb}$ , and large inputs of  $^{137}\text{Cs}$  and  $^{239,240}\text{Pu}$  from Yangtze River's drainage basin. © 1999 Elsevier Science B.V. All rights reserved.

**Keywords:** sedimentation; East China Sea;  $^{210}\text{Pb}$ ;  $^{137}\text{Cs}$ ; plutonium

## 1. Introduction

The East China Sea (ECS) is a broad and shallow epicontinental sea between mainland China in the west, the Kuroshio Current (KC) in the east, Taiwan and the Taiwan Strait in the south, and the Yellow Sea in the north (Fig. 1). Circulation in the ECS is dominated by the northward flow of the KC along the edge of the ECS shelf and the Taiwan Warm Current (TWC) in the midshelf. Both the KC and the

TWC have high salinity and warmer temperature. In contrast, the Changjiang (i.e., the Yangtze River) Cold Water (CJCW) has lower salinity and temperature and flows southward near the bottom along the coast of mainland China (Milliman et al., 1989). Associated with the major currents are high tidal currents, extremely high sediment supply, frequent and intense storm events and thus re-suspension of sediments. These physical features and processes make the ECS one of the most dynamic marginal seas in the world.

The two major sediment dispersal systems in the ECS are the proximal portion of the Yangtze River and the distal portion of the Yellow River (Huanghe).

\* Corresponding author. Fax: +886-2-2783-9871; E-mail: huh@earth.sinica.edu.tw

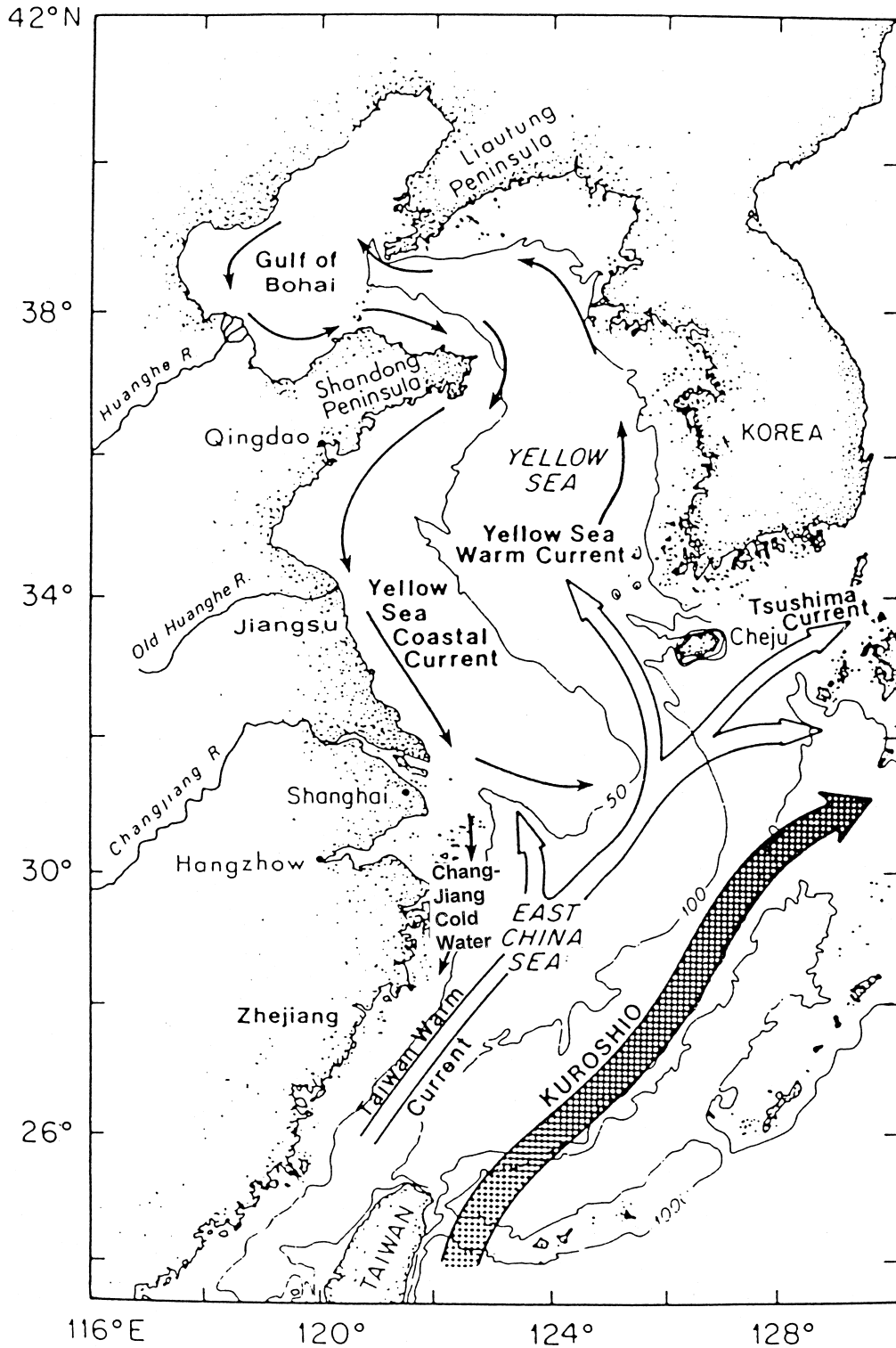


Fig. 1. Schematic of regional circulation in the East China and Yellow Seas.

These two largest rivers in China are among the top four of the world's rivers in terms of sediment discharge. The Yellow River annually discharges  $\sim 1 \times 10^9$  ton of sediment into the Gulf of Bohai (Milliman and Meade, 1983). It was reported (Lee and Chough, 1989; Zhang, 1996) that only a small portion of this sediment load is transported southward by the Yellow Sea Coastal Current (YSCC). Near the mouth of the Yangtze River (at  $\sim 32^\circ\text{N}$ ), the YSCC divides into two branches; one flows offshore toward the southeast and the other merges into the CJCW flowing farther south along the coastline (Fig. 1). It is estimated that  $< 2\%$  of the sediment discharged by the Yellow River can be accounted for in an offshore mud patch to the north of  $30^\circ\text{N}$  (DeMaster et al., 1985). Yet unclear, though, is how much Yellow River sediments is transported nearshore to the south of  $30^\circ\text{N}$ .

The Yangtze River annually discharges  $\sim 5 \times 10^8$  ton of sediments directly into the ECS (Milliman and Meade, 1983). According to DeMaster et al. (1985), approximately 40% of the sediment transported by the Yangtze River is deposited in the inner shelf north of  $30^\circ\text{N}$ . If so, the remaining 60% must be transported offshore by the YSCC and to the south of  $30^\circ\text{N}$  by the CJCW.

Besides sediments discharged by the Yangtze and the Yellow Rivers, erosion from Taiwan constitutes yet another significant source of sediments to the ECS. With denudation and erosion rates among the highest in the world (Li, 1976), the island of Taiwan yields  $\sim 2.6 \times 10^8$  ton of sediments annually; most of which are delivered westward by rivers toward the Taiwan Strait (Water Resources Planning Commission, 1996). Compared with the above three major sources, other smaller rivers along the coast of mainland China are insignificant contributors of sediments to the ECS (Yanagi et al., 1997).

The pathways and fates of suspended and settling particles in the ECS have direct bearing on the mass balance and fluxes of chemical materials in this marginal sea. For example, an issue of prime importance but as yet unresolved is whether coastal seas are sources or sinks of  $\text{CO}_2$  (Kempe, 1995) and other anthropogenic materials. As a marginal sea bordering the most populated region in the world and separated from the largest ocean (i.e., the Pacific) by the strongest western boundary current (i.e., the

Kuroshio), the ECS is identified by the KEEP (Kuroshio Edge Exchange Processes) project as a test ground to address this problem. However, it is not possible to calculate the budgets of carbon and other chemical materials in the ECS without adequate constraints on their benthic fluxes, including fluxes associated with burial and post-depositional sediment redistribution. As a component of KEEP, our task is to study the accumulation and transport of sediments in the ECS using fallout radionuclides  $^{210}\text{Pb}$ ,  $^{137}\text{Cs}$  and  $^{239,240}\text{Pu}$  as tracers.

With a half-life of 22.3 years and well-defined source functions,  $^{210}\text{Pb}$  is the most commonly used chronometer for estimating sedimentation rates in near-shore environments (Appleby and Oldfield, 1992, and references therein). Based on  $^{210}\text{Pb}$  profiling, DeMaster et al. (1985) obtained accumulation rates up to  $5.4 \text{ cm yr}^{-1}$  near the mouth of the Yangtze River, from  $< 0.1$  to  $0.2 \text{ cm yr}^{-1}$  in a stretch of fine sandy deposits away from the Yangtze River, and  $\sim 0.3 \text{ cm yr}^{-1}$  in a mud patch about 400 km offshore. In the same offshore area mentioned above, higher sedimentation rates, ranging from 0.2 to  $0.8 \text{ cm yr}^{-1}$ , were reported by Huang et al. (1983) and Su et al. (1983). In the southern ECS around Taiwan, sedimentation rates ranging from 0.06 to  $0.87 \text{ cm yr}^{-1}$  were measured over some shelf area and on the lower continental slope between Taiwan and the South Okinawa Trough (Narita et al., 1990; Chen, 1995; Chung and Chang, 1995). Besides, there are also areas of no net sediment accumulation, especially in the mid-shelf and the slope regions (Chen, 1995; Chung and Chang, 1995).

Although the data summarized above are not scant, they are still sketchy. To fill obvious gaps, we have collected a suite of cores from various physiographic settings (Fig. 2) and analyzed them for  $^{210}\text{Pb}$ . With the expanded database, we hope to delineate spatial variation of sediment accumulation in the ECS, and to obtain more representative values for mass balance considerations. In addition, by comparing  $^{210}\text{Pb}$  inventories between cores and with values expected from known input sources, we wish to distinguish between areas of no net sedimentation and areas of sediment focusing.

While using  $^{210}\text{Pb}$  data alone, caution must be taken. Due to tidal currents, storms and bioturbation, estuarine and shelf sediments are readily subjected to

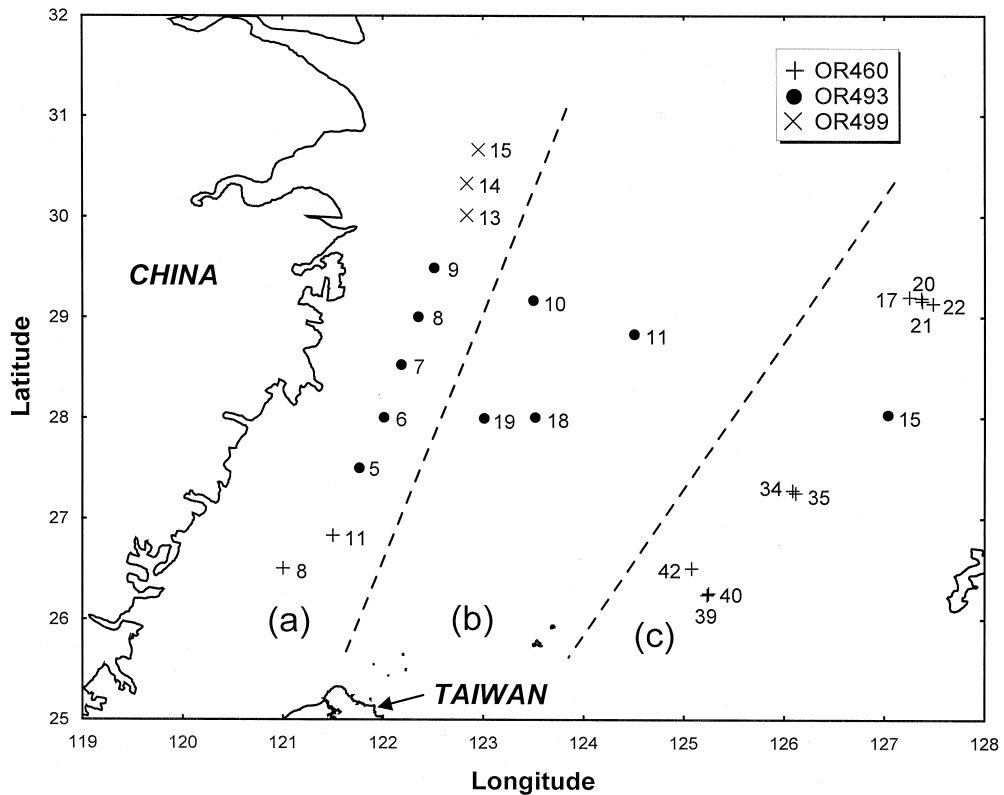


Fig. 2. Map showing locations of sediment cores used in this study. To facilitate the presentation of subsequent figures, the cores are divided into three groups based on location as well as bathymetry of the sampling sites: (a) the inner shelf, (b) the mid-shelf, and (c) the outer-shelf and slope regions.

mixing. Therefore, sedimentation rates derived from  $^{210}\text{Pb}$  may be overestimated. To constrain  $^{210}\text{Pb}$ -based sedimentation rates, distributions of  $^{137}\text{Cs}$  and  $\text{Pu}$  are also measured. As will be shown later, profiles of these two nuclides in sediments often reflect the history of nuclear fallout, thus enabling us to establish sediment chronology independently.

In addition to the determination of sedimentation rates, profiles and inventories of all three nuclides will be used to shed light on mixing and redistribution of sediments and chemical scavenging of these nuclides.

## 2. Materials and methods

Subcores were taken and processed on board R/V *Ocean Researcher-I* immediately following the re-

covery of box cores. Cores were extruded vertically with a hydraulic jack and sampled at 1–2 cm intervals. The outer rim (~0.5 cm) of each sediment slab was trimmed off to avoid contamination between layers. The sectioned samples were sealed and kept frozen until further processing in the home laboratory. Based on weight loss after freeze-drying, the water content of the wet sediments was calculated. A correction for the amount of salt retained in the dry sediments was made based on the water content and the salinity of the bottom water. Activities and inventories of nuclides and mass accumulation rates reported in this paper are based on salt-free basis.

Determination of  $^{210}\text{Pb}$  (via  $^{210}\text{Po}$ ) and  $^{239,240}\text{Pu}$  by  $\alpha$ -spectrometry was performed separately using 2 g (for  $^{210}\text{Pb}$ ) or 10 g (for  $^{239,240}\text{Pu}$ ) of dried sediment samples.  $^{209}\text{Po}$  and  $^{242}\text{Pu}$  obtained from ORNL were

added as the yield determinants prior to sample digestion. The  $^{209}\text{Po}$  and  $^{242}\text{Pu}$  spikes have been calibrated vs. NIST-certified  $^{208}\text{Po}$  (SRM-4327) and  $^{244}\text{Pu}$  (SRM-996), respectively. Polonium isotopes were plated onto a silver disc from the sample solution (in 1.5 N HCl, in the presence of ascorbic acid) at 80–90°C for ~2 h. Isotopes of Pu were electroplated onto stainless steel discs. The counting results were corrected for the decay of  $^{210}\text{Po}$  (from the time of plating to counting) and  $^{210}\text{Pb}$  (from sample collection to Po plating). More detailed description of the radiochemical procedures can be found elsewhere (Huh et al., 1987, 1990, 1996).

$^{214}\text{Pb}$  (a precursor of  $^{210}\text{Pb}$  and used as an index of supported  $^{210}\text{Pb}$ ) and  $^{137}\text{Cs}$  were measured by  $\gamma$ -spectrometry based on photon energies at 351.99 keV and 661.62 keV, respectively. The counting system is equipped with a 150% efficiency (relative to  $3 \times 3$  NaI) HPGe detector (EG&G ORTEC GEM-150230) interfaced to a digital gamma-ray spectrometer (DSPEC<sup>®</sup>). The detector was calibrated using NIST SRM 4353 (Rocky Flats soil) and 4350B (Columbia River sediments), and IAEA standard SD-N-1 (Irish Sea sediments). At 661.62 keV, the absolute counting efficiency for our samples (contained in 8.5-cm diameter plastic jars) varied from 6.33% for 10-g samples to 4.32% for 100-g samples, and the peak resolution was 1.21 keV (FWHM) with a peak-to-Compton ratio higher than 90.

### 3. Results and discussion

Space limitation does not allow us to list the nuclide activity data in its entirety, but they can be provided upon request. For the following discussion, all nuclide activities and the derived parameters are plotted in figures.

#### 3.1. $^{210}\text{Pb}$ -derived apparent sedimentation rates

Strictly speaking, sedimentation rates calculated from gradients of excess  $^{210}\text{Pb}$  (i.e.,  $^{210}\text{Pb}_{\text{ex}}$ ) are valid only if the sediment column is not disturbed and the distribution of  $^{210}\text{Pb}$  is at steady state. However, this ideal condition is not common, especially in a dynamic environment like the ECS. Therefore, before the extent of sediment mixing can be assessed, it is more conservative to refer to  $^{210}\text{Pb}$ -based

sedimentation rates as ‘apparent’ (i.e., ‘at first sight’) values.

To facilitate the following discussion, the sediment profiles of  $^{210}\text{Pb}_{\text{ex}}$  (along with  $^{137}\text{Cs}$  and  $^{239,240}\text{Pu}$ ) are arranged in three groups based on location and bathymetry of the coring sites: the inner shelf (Fig. 3a), the midshelf (Fig. 3b), and the outer shelf and the continental slope regions (Fig. 3c). Eight of the 12 inner and mid-shelf cores show much reduced  $^{210}\text{Pb}$  gradients in the upper sediment column. Considering the presence of benthic organisms (hence bioturbation) and bottom currents, it is most likely that the slope changes are caused by sediment mixing. Otherwise, if it were not due to sediment mixing, these profiles would be explained by an increase of sedimentation rate by factors of more than four during the past 1–2 decades or so. The possibility of such a drastic increase in sedimentation rates can be ruled out by the  $^{137}\text{Cs}$  and Pu data (to be discussed later).

In contrast to the shelf cores, profiles of  $^{210}\text{Pb}_{\text{ex}}$  in all slope cores from water depths between 400–1000 m show simple exponential decrease throughout the length of the cores (Fig. 3c). Although there is no direct evidence of sediment mixing based on  $^{210}\text{Pb}$  data alone, Pu data (discussed below) do suggest sediment mixing. Therefore,  $^{210}\text{Pb}_{\text{ex}}$ -based apparent sedimentation rates over the slope, which vary between 0.06–0.09  $\text{cm yr}^{-1}$ , should also be taken as upper limits.

In two cores (460-22 and 460-39) collected further offshore from water depths of  $\geq 1000$  m (Fig. 3c),  $^{210}\text{Pb}_{\text{ex}}$  profiles show changes in gradient at ~5 cm. Apparent sedimentation rates based on lower sections of the profiles (0.023 and 0.047  $\text{cm yr}^{-1}$ , respectively) are closer to  $^{137}\text{Cs}$  or Pu-derived sedimentation rates, thus suggesting that upper parts of these cores have also been subjected to mixing.

#### 3.2. Sedimentation rates deduced from profiles of $^{137}\text{Cs}$ and $^{239,240}\text{Pu}$

As a result of atmospheric nuclear tests,  $^{137}\text{Cs}$  and Pu isotopes started to appear in environmental samples at measurable levels from the early 1950s. Atmospheric fluxes of these fallout nuclides then followed the variation of activities released from nuclear detonations, which peaked in 1963 and de-

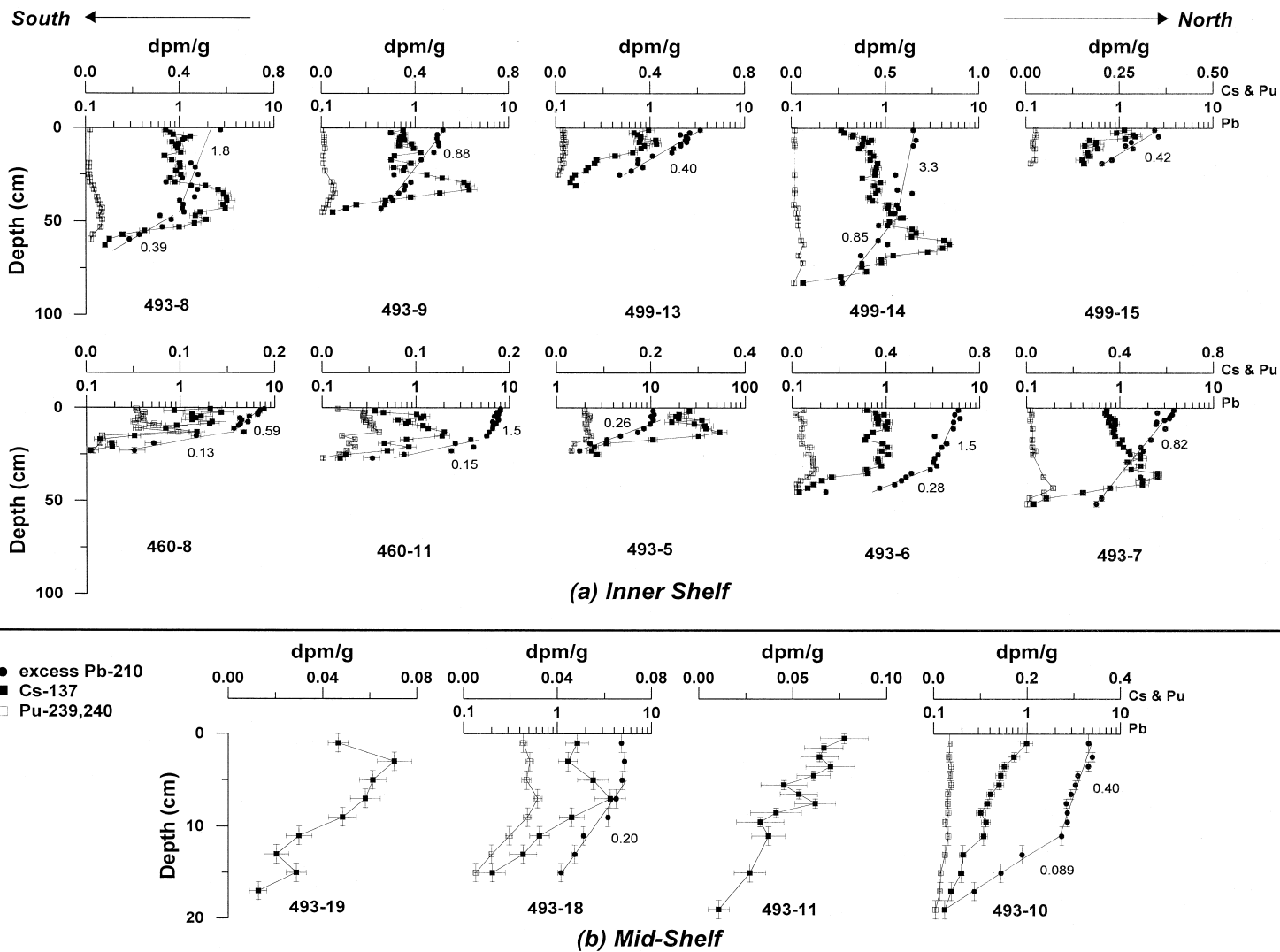


Fig. 3. Profiles of excess  $^{210}\text{Pb}$ ,  $^{137}\text{Cs}$  and  $^{239,240}\text{Pu}$  in (a) the inner shelf, (b) the mid-shelf, and (c) the outer-shelf and slope regions. Each profile is identified with a three-digit cruise number (i.e., cruises 460, 493 and 499 of R/V *Ocean Researcher-1*) followed by a box core number. Numbers next to the regression lines are  $^{210}\text{Pb}$ -based apparent sedimentation rates (in  $\text{cm yr}^{-1}$ ).

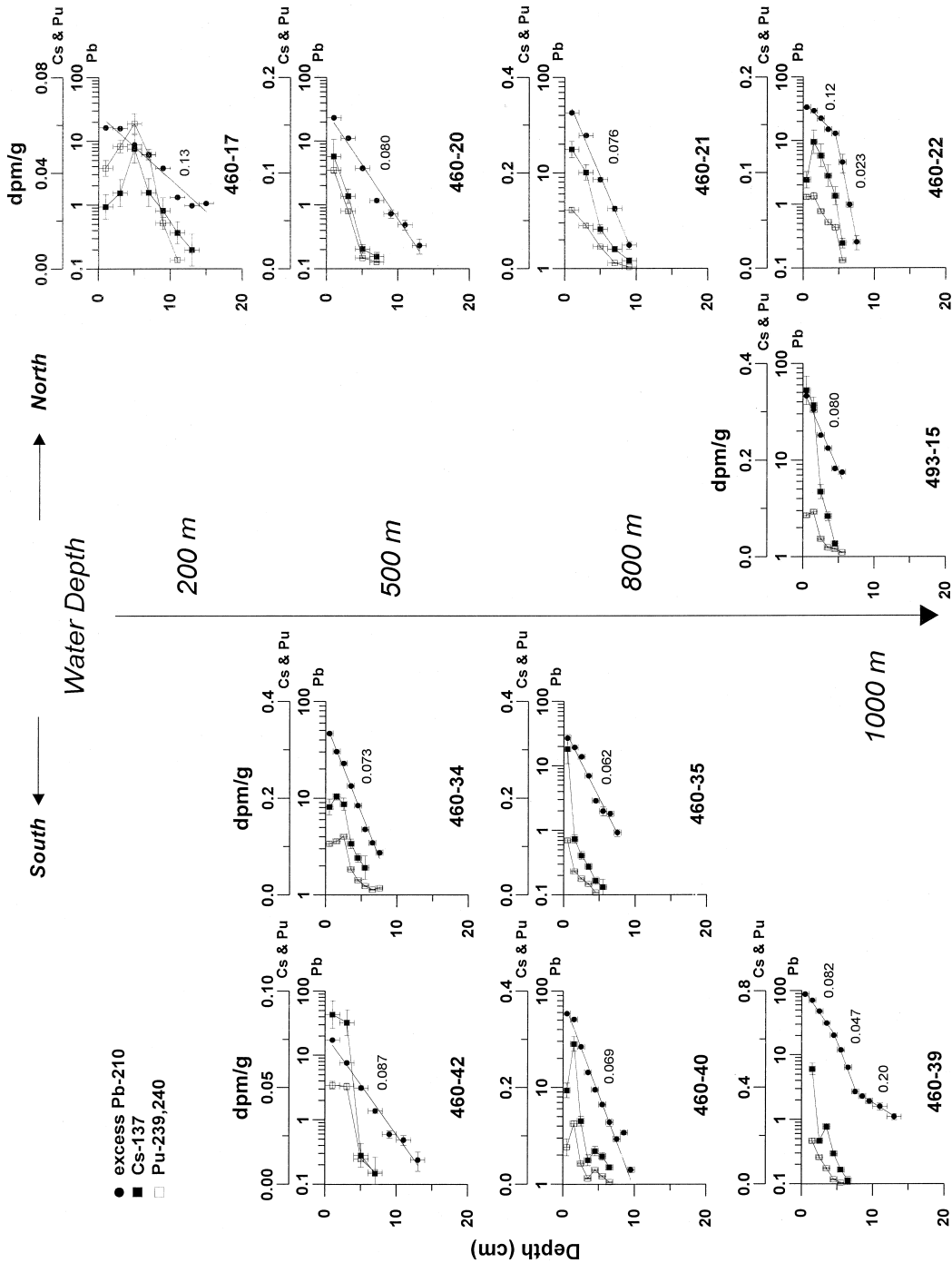


Fig. 3 (continued).

creased sharply after the enactment of the Test-Ban Treaty in the same year. Profiles of  $^{137}\text{Cs}$  and  $^{239,240}\text{Pu}$  (Fig. 3) generally conform to the history of nuclear fallout in showing an upward increase at the lower parts of all cores and a subsurface maximum in some cores. However, in some cores, the penetration depth of  $^{137}\text{Cs}$  is deeper than what would be anticipated from the subsurface radiocesium peak, suggesting post-depositional mobilization of particle-bound  $^{137}\text{Cs}$ . This may be caused by ion exchange with  $\text{NH}_4^+$  which reaches high concentrations in anoxic pore waters at depth (Comans et al., 1989).

Whether or not the subsurface maximum can be seen depends to a large extent on sediment accumulation rates (hence the achievable sampling resolution); it can be more easily observed in inner shelf sediments with more rapid accumulation rates than in slope cores with much slower sedimentation rates.

If direct fallout from the atmosphere above the ECS is the sole source of  $^{137}\text{Cs}$  and Pu to sediments and surficial sediments are not mixed, then both nuclides should exist at very low or undetectable levels above the 1963 peak. This scenario can be immediately dismissed because activities of these nuclides in the upper sediment column are too high to back up the assumption. However, mixing alone cannot fully account for the distribution of either nuclide in the cores, especially near the estuary where inventories of  $^{137}\text{Cs}$  above the subsurface peak are much more than that can be expected from direct atmospheric input. To account for the discrepancy, it is necessary to invoke delayed input of additional  $^{137}\text{Cs}$  eroded from Yangtze River's drainage basin.

Although mixing and drainage basin inputs can modify the shape and gradient of  $^{137}\text{Cs}$  and Pu profiles, the position of the subsurface peak is to a large extent controlled by sediment burial (Miller and Heit, 1986). Whether or not the subsurface maximum can be seen depends to a large extent on sediment accumulation rates (hence the achievable sampling resolution); it can be more easily observed in inner shelf sediments with more rapid accumulation rates than in slope cores with much slower sedimentation rates. To the extent that the subsurface peak is discernible, it may be a useful time marker for 1963.

With the time of core collection assigned to the core tops and 1963 to the depths of the subsurface

$^{137}\text{Cs}$  or  $^{239,240}\text{Pu}$  peaks, sedimentation rates for the studied cores are calculated where feasible. The results are compared with  $^{210}\text{Pb}$ -derived sedimentation rates. It is important to note that, when  $^{210}\text{Pb}$ -based and  $^{137}\text{Cs}$ -based sedimentation rates do not agree well, the former tends to be higher than the latter (by 53% on average). In other words, the  $^{210}\text{Pb}$  dating method appears to be more susceptible to sediment mixing in our study area.

Fig. 4 shows spatial variation of  $^{137}\text{Cs}$ -based apparent sedimentation rates which vary from  $> 1 \text{ cm yr}^{-1}$  near the Yangtze River estuary to  $< 0.1 \text{ cm yr}^{-1}$  beyond the shelf break. Although these rates are not free from errors (to be further discussed later), a first-order picture of the pathways of sediment transport can be gleaned from the map. There is a general decrease of sedimentation rates with distance offshore and southward from the Yangtze River estuary along shore. This pattern is consistent with the dispersal of sediments by the current and tidal systems.

### 3.3. An evaluation of sediment mixing rates using a diffusion-decay model

With sedimentation rates constrained by the subsurface  $^{137}\text{Cs}$  and Pu maximum, it may be possible to make first order calculations of mixing rates from the  $^{210}\text{Pb}$  profiles. If sedimentation and mixing rates are assumed to be constant in the upper sediment column where  $^{210}\text{Pb}_{\text{ex}}$  decreases with depth in an exponential-like manner, the distribution of  $^{210}\text{Pb}_{\text{ex}}$  can be described by:

$$D \frac{\partial^2 C}{\partial Z^2} - S \frac{\partial C}{\partial Z} - \lambda C = 0$$

where  $Z$  is depth below the core top,  $C$  is the activity of  $^{210}\text{Pb}_{\text{ex}}$  at depth  $Z$ ,  $D$  is mixing coefficient,  $S$  is sedimentation rate, and  $\lambda$  is the decay constant ( $0.0311 \text{ yr}^{-1}$ ) of  $^{210}\text{Pb}$ . With the boundary conditions that  $C = C_0$  at  $Z = 0$ , and  $C = 0$  as  $Z \rightarrow \infty$ , the solution for  $C$  is:

$$C = C_0 \exp\left(\frac{S - \sqrt{S^2 + 4\lambda D}}{2D} Z\right)$$

The value of the exponent in the above equation can be determined from the slope of the straight line on a

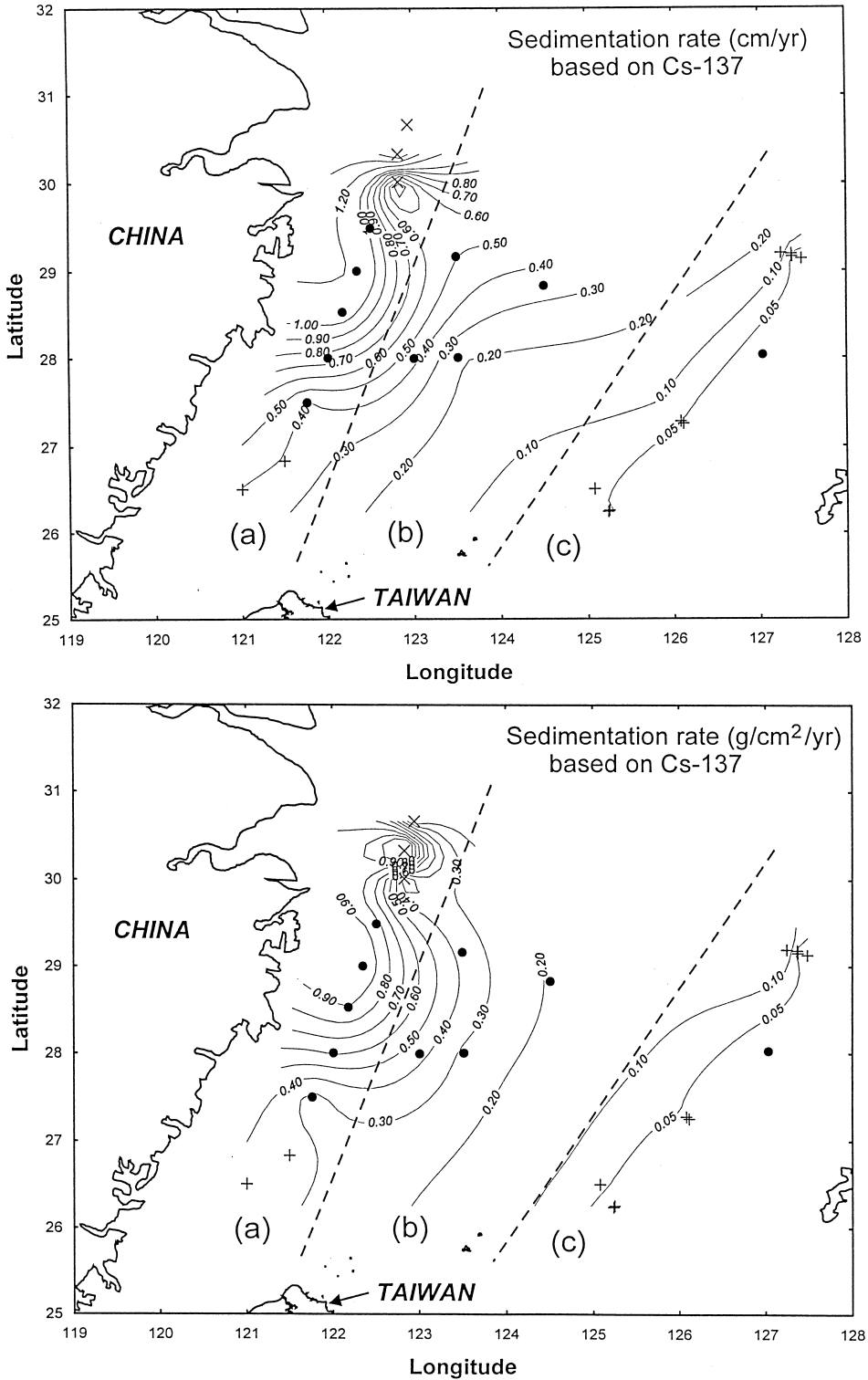


Fig. 4. Spatial variation of linear sedimentation rates (upper panel) and mass accumulation rates (lower panel) estimated from <sup>137</sup>Cs profiles.

semi-log (i.e.,  $\ln C$  vs.  $Z$ ) plot. Therefore, if  $S$  is given (i.e., based on  $^{137}\text{Cs}$  or  $\text{Pu}$ ),  $D$  can be calculated.  $D$ -values thus obtained from inner-shelf cores fall within 2–50  $\text{cm}^2 \text{yr}^{-1}$  (averaging  $\sim 20 \text{cm}^2 \text{yr}^{-1}$ ). Mixing rates of this magnitude are consistent with typical values for near-shore silty clay sediments (Aller, 1977; Turekian et al., 1978). As for the core from the outer shelf (core 460-17) and those beyond the shelf break, the calculated mixing rates vary between 0.03–0.3  $\text{cm}^2 \text{yr}^{-1}$  (averaging  $\sim 0.2 \text{cm}^2 \text{yr}^{-1}$ ), which are lower than those obtained for inner shelf cores by two orders of magnitude on average.

### 3.4. Atmospheric fluxes of $^{210}\text{Pb}$ , $^{137}\text{Cs}$ and $^{239,240}\text{Pu}$ in the East China Sea

In order to interpret the observed inventories of  $^{210}\text{Pb}$ ,  $^{137}\text{Cs}$  and  $^{239,240}\text{Pu}$  in sediments with reference to nuclide behaviors and sedimentation dynamics, it is necessary to quantify their atmospheric fluxes and expected cumulative fallout. For  $^{210}\text{Pb}$ , however, atmospheric fallout is not its only source; in-situ production (from  $^{226}\text{Ra}$  decay) constitutes another source for this nuclide in marine environments. The relative importance of these two sources in the ECS shelf can be evaluated as follows. Given a water depth of 200 m and a mean  $^{226}\text{Ra}$  concentration of 0.1  $\text{dpm l}^{-1}$  (Yeh and Chung, 1997), the production rate of  $^{210}\text{Pb}$  in the water column is 0.06  $\text{dpm cm}^{-2} \text{yr}^{-1}$ . The atmospheric  $^{210}\text{Pb}$  flux is estimated to be 2  $\text{dpm cm}^{-2} \text{yr}^{-1}$  in the western North Pacific area near Japan (Nozaki and Tsunogai, 1973); 1.6  $\text{dpm cm}^{-2} \text{yr}^{-1}$  at Naha City on Okinawa (Tsunogai et al., 1985); 1.8  $\text{dpm cm}^{-2} \text{yr}^{-1}$  near Hangzhou, China (DeMaster et al., 1985); and 1.9  $\text{dpm cm}^{-2} \text{yr}^{-1}$  at the Sun–Moon Lake in middle Taiwan (Huh et al., 1996). Considering the difference in sampling methods and uncertainties involved in the measurements, these values are remarkably similar. Situated well within the above-referenced sites, the ECS is in all likelihood receiving a similar  $^{210}\text{Pb}$  flux. Therefore, it is fair to say that atmospheric fallout is the dominant source of  $^{210}\text{Pb}$  in the ECS. Taking 1.8  $\text{dpm cm}^{-2} \text{yr}^{-1}$  as the atmospheric  $^{210}\text{Pb}$  flux and 0.06  $\text{dpm cm}^{-2} \text{yr}^{-1}$  as the production rate of  $^{210}\text{Pb}$  in the water column, the inventory of excess  $^{210}\text{Pb}$  in sediments that can be

sustained by the total flux is  $\sim 60 \text{dpm cm}^{-2}$  at steady state.

Atmospheric fluxes of  $^{137}\text{Cs}$  and  $^{239,240}\text{Pu}$  from global fallout depend primarily on latitude. Over the ECS Shelf, they can be evaluated as follows. Based on soil profiles, Hardy et al. (1973) reported that the cumulative fallout of  $^{239,240}\text{Pu}$  in the 20–30°N latitudinal band was 0.21  $\text{dpm cm}^{-2}$  as of 1971. We are not aware of any updated data since then, but it can be estimated indirectly via other fallout nuclides as follows. If the integrated  $^{90}\text{Sr}$  fallout in the same latitudinal band as of 1981 (10.6  $\text{dpm cm}^{-2}$ ) reported 10 years later (United Nations Scientific Committee on the Effects of Atomic Radiation, 1982) is divided by the  $^{90}\text{Sr}/^{239,240}\text{Pu}$  activity ratio in fresh stratospheric or tropospheric debris (= 56; Sholkovitz, 1983), the resulting cumulative fallout of  $^{239,240}\text{Pu}$  is 0.19  $\text{dpm cm}^{-2}$ . Considering the uncertainties involved between the two approaches, the agreement is fairly good and suggests that nuclear fallout has been trivial since 1971.

The time series record of global-fallout of  $^{137}\text{Cs}$  should be the same as that of  $^{239,240}\text{Pu}$ . Since the  $^{137}\text{Cs}/^{90}\text{Sr}$  activity ratio is essentially constant ( $\approx 1.5$ ) in fresh bomb debris, cumulative fallout of  $^{137}\text{Cs}$  can be calculated by multiplying this ratio with the cumulative fallout of  $^{90}\text{Sr}$ , i.e.,  $1.5 \times 10.6 \text{dpm cm}^{-2} = 15.9 \text{dpm cm}^{-2}$ . If the time series of  $^{137}\text{Cs}$  is decay-corrected to January 1998, this value reduces to 7.1  $\text{dpm cm}^{-2}$ .

In the section to follow, inventories of 60, 7.1 and 0.21  $\text{dpm cm}^{-2}$ , as derived above, will be used as the reference values for  $^{210}\text{Pb}$ ,  $^{137}\text{Cs}$  and  $^{239,240}\text{Pu}$ , respectively, to address sediment transport and chemical scavenging in the ECS shelf.

### 3.5. Sediment inventories of excess $^{210}\text{Pb}$ , $^{137}\text{Cs}$ and $^{239,240}\text{Pu}$ : implications for sediment transport and chemical scavenging

Fig. 5 shows spatial variations of  $^{210}\text{Pb}_{\text{ex}}$ ,  $^{137}\text{Cs}$  and  $^{239,240}\text{Pu}$  inventories in the sediments of the ECS. Inventories of  $^{210}\text{Pb}_{\text{ex}}$  in the studied cores (Fig. 5a) vary between 32–140  $\text{dpm cm}^{-2}$  (averaging 76  $\text{dpm cm}^{-2}$ ) and increase towards the south in the inner- and mid-shelf areas. Based on our data, the overall standing stock of  $^{210}\text{Pb}_{\text{ex}}$  in ECS sediments is about 25% higher than the value (60  $\text{dpm cm}^{-2}$ )

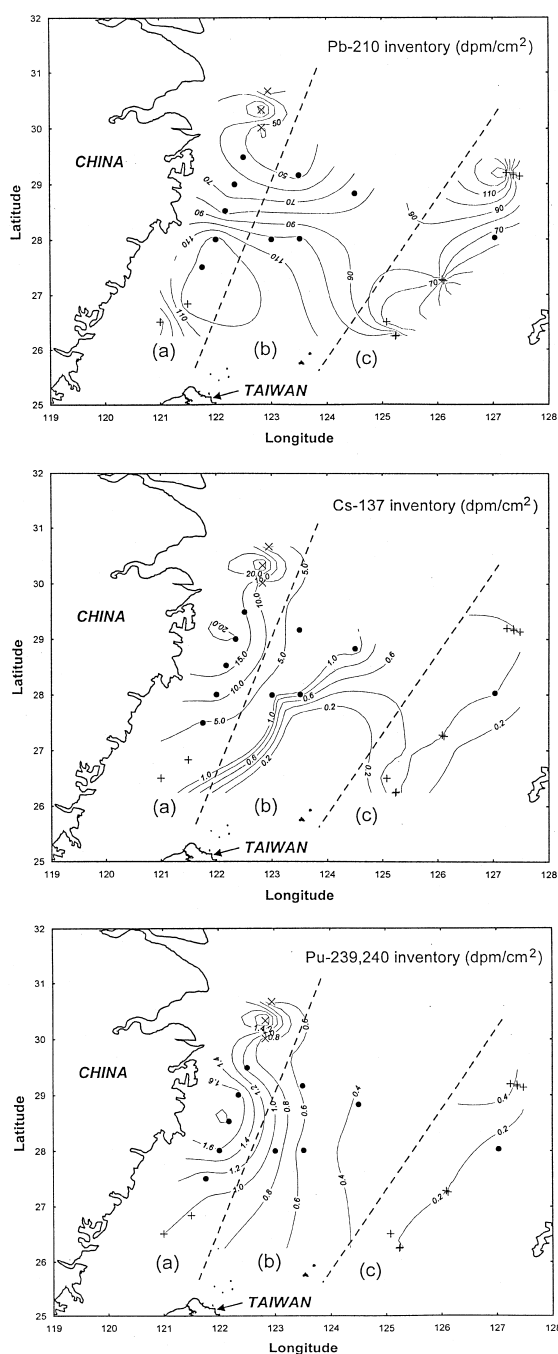


Fig. 5. Spatial distribution of (from top to bottom)  $^{210}\text{Pb}_{\text{ex}}$ ,  $^{137}\text{Cs}$  and  $^{239,240}\text{Pu}$  inventories in East China Sea sediments.

expected from direct atmospheric input and in-situ production. In light of the lack of  $^{210}\text{Pb}_{\text{ex}}$  enrichment

in estuarine sediments, wash-in from the drainage basin is unimportant for this nuclide. The additional  $^{210}\text{Pb}$  inventory is probably caused by lateral input of open ocean waters from the south followed by enhanced scavenging at this marginal sea (i.e., the so-called boundary scavenging).

The measured  $^{137}\text{Cs}$  inventories span two orders of magnitude (Fig. 5b), from  $0.26 \text{ dpm cm}^{-2}$  in the slope area (core 460-35) to  $33 \text{ dpm cm}^{-2}$  near the Hangzhou Bay (i.e., core 499-14). In the study area,  $^{137}\text{Cs}$  inventories higher than the reference value of  $7.1 \text{ dpm cm}^{-2}$  are restricted to the inner shelf area extending  $\sim 400 \text{ km}$  to the south from the mouth of the Yangtze River and  $\sim 200 \text{ km}$  offshore. This pattern clearly points to the estuarine source for the excess  $^{137}\text{Cs}$ . The clay-sized sediments in this area are dominated by illite ( $> 70\%$ ) with high cation exchange capacity (hence the ability to adsorb  $^{137}\text{Cs}$ ). It is also there that the sediments are most enriched in other anthropogenic pollutants such as Pb discharged from the Yangtze River (Huh and Chen, 1999). Out of this area, sediment inventories of  $^{137}\text{Cs}$  generally decrease southward along shore and eastward offshore. Beyond the shelf break ( $> 200 \text{ m}$ ), the observed  $^{137}\text{Cs}$  inventories are less than 10% of the reference value, indicating that  $> 90\%$  of the  $^{137}\text{Cs}$  precipitated directly from the atmosphere still exists in the overlying water or has been transported away from the shelf.

The distribution of  $^{239,240}\text{Pu}$  inventory (Fig. 5c) is similar to that of  $^{137}\text{Cs}$ , with the highest values occurring at exactly the same area and lower values offshore. However, the observed sediment inventories of  $^{239,240}\text{Pu}$  in the entire shelf are higher than the inventory expected from direct atmospheric fallout. Only beyond the shelf break at water depths deeper than  $800 \text{ m}$  are lower  $^{239,240}\text{Pu}$  inventories (i.e.,  $< 0.21 \text{ dpm cm}^{-2}$ ) found. This reflects the fact that, compared with  $^{137}\text{Cs}$ , Pu has much higher affinity for particles and therefore can be more easily scavenged from the water column.

### 3.6. Sediment budget in the East China Sea shelf—what is the missing link?

Sediment budget in the ECS Shelf is controlled by input from the adjacent lands, accumulation on the shelf, and output to the open Pacific. Of the three

terms, the input term is relatively well-quantified. In comparison, it is almost impossible to measure the output term unless the exits and sinks of sediments are well-defined. This study is focused at the accumulation term to constrain the mass balance of sediments in the ECS Shelf.

The area of the ECS shelf (water depth < 200 m) between 31.5°N and 24°N is approximately  $5 \times 10^5$  km<sup>2</sup>. If sediments discharged from the Yangtze River as well as those eroded from Taiwan were evenly distributed over this area without any export to the open ocean, the resulting sedimentation rate would be 0.14 g cm<sup>-2</sup> yr<sup>-1</sup>. Based on Fig. 4b, however, the integrated mean sedimentation rate would be  $\sim 0.3$  g cm<sup>-2</sup> yr<sup>-1</sup>. The difference can be reconciled or reduced by considering the possibility of additional sediment source to the ECS shelf and the effect of sediment mixing. These are discussed below.

If the apparent imbalance of sediment budget is caused by an underestimate of sediment input to the ECS shelf, then we should consider the probable role of the Yellow River dispersal system. Based on previous studies (Lee and Chough, 1989; Zhang, 1996), of the  $\sim 11 \times 10^8$  ton of sediments discharged from the Yellow River annually, about 65% is deposited in the Gulf of Bohai and 20% in the Yellow Sea. If these percentages are accurate, then the remaining 15% of the sediments are most likely carried southward to the ECS by the YSCC. By invoking this additional input, the mean sedimentation rate in the ECS shelf would be adjusted to 0.17 g cm<sup>-2</sup> yr<sup>-1</sup>. This revised value is not much higher than 0.14 g cm<sup>-2</sup> yr<sup>-1</sup> but still substantially lower than 0.3 g cm<sup>-2</sup> yr<sup>-1</sup>. In other words, the Yellow River dispersal system has only a minor effect on the sediment budget in our study area.

The other possibility for the large discrepancy between sediment input and deposition is that we have overestimated sedimentation rates. Although we contend that sedimentation rates estimated from <sup>137</sup>Cs are more reliable than those based on <sup>210</sup>Pb, profiles of both nuclides are affected by sediment mixing. If an impulse tracer such as the 1963 fallout peak is subjected to 'box-model-type' mixing at core top right after deposition, the tracer is immediately mixed downward into the bottom of the mixed layer, and then subsequently mixed upward with the overlying

sediment as it is deposited. As a result the lower contact remains sharp, but reduced in contrast, while the upper boundary becomes gradational (Ruddiman and Glover, 1972; Guinasso and Schink, 1975). In this extreme case, if the tracer is used as a time marker to determine sedimentation rate, it is necessary to subtract the thickness of the mixed layer from the depth of the subsurface peak. Ideally, mixed layer of this type and its thickness can be determined from <sup>210</sup>Pb profiles showing no concentration gradients in the core top. In this study, with the exception of only two cores (493-5 from the inner shelf and 493-18 from the mid-shelf), no other cores show this type of mixing. Therefore, we could not perform the mixed-layer depth correction for the entire study area and the sedimentation rates plotted on Fig. 4b should be taken as upper limits.

#### 4. Conclusions

Sediment cores collected from various settings in the ECS were analyzed for <sup>210</sup>Pb, <sup>137</sup>Cs and <sup>239,240</sup>Pu to derive rates of sediment accumulation and mixing, delineate the pathways of sediment transport, and assess budgets of these nuclides and sediments in this marginal sea.

Sedimentation rates derived from profiles of <sup>210</sup>Pb<sub>ex</sub> are higher than those based on <sup>137</sup>Cs and <sup>239,240</sup>Pu by 53% on average, suggesting that the <sup>210</sup>Pb<sub>ex</sub> method is more susceptible to sediment mixing. The more reasonable sedimentation rates based on <sup>137</sup>Cs vary from  $\sim 2$  cm yr<sup>-1</sup> to  $< 0.1$  cm yr<sup>-1</sup> and generally decrease southward from the Yangtze River estuary and eastward toward the open ocean. This pattern is consistent with the point of input and expected pathways of sediment transport by the current and tidal systems. Although the rates of sediment input to the ECS and accumulation on the shelf can be estimated, it is still not possible to evaluate the export of sediments out of this marginal sea. A better understanding of sediment redistribution and mixing in the ECS is required to address this issue.

With apparent sedimentation rates obtained, an attempt was made to evaluate sediment mixing using a diffusion-decay model. The calculated mixing coefficients average  $\sim 2$  cm<sup>2</sup> yr<sup>-1</sup> based on inner

shelf cores and  $\sim 0.2 \text{ cm}^2 \text{ yr}^{-1}$  for outer shelf and slope cores.

Inventories of  $^{210}\text{Pb}_{\text{ex}}$  in sediments of the ECS shelf vary between 32–140  $\text{dpm cm}^{-2}$  and generally increase towards the south in the inner- and mid-shelf areas. The mean  $^{210}\text{Pb}_{\text{ex}}$  inventory (76  $\text{dpm cm}^{-2}$ ) is  $\sim 25\%$  higher than that can be sustained by atmospheric input and water column production at steady state. The spatial variation can be explained by sediment re-distribution coupled with boundary scavenging of  $^{210}\text{Pb}$  in waters advected from the south.

Sediment inventories of  $^{137}\text{Cs}$  span two orders of magnitude, from 0.26 to 33  $\text{dpm cm}^{-2}$ , and decrease distinctly from the Yangtze River estuary southward along shore and eastward offshore.  $^{137}\text{Cs}$  inventories higher than that expected from cumulative fallout (ca. 7.1  $\text{dpm cm}^{-2}$ ) are restricted to the estuary and inner shelf region receiving large inputs from the Yangtze River's drainage basin. Elsewhere in the ECS, sediment inventories of  $^{137}\text{Cs}$  are much less than 7.1  $\text{dpm cm}^{-2}$ , indicating that most  $^{137}\text{Cs}$  precipitated directly from the atmosphere still resides in the water column.

The distribution of  $^{239,240}\text{Pu}$  inventory is similar to that of  $^{137}\text{Cs}$ . However, the observed sediment inventories of  $^{239,240}\text{Pu}$  everywhere on the shelf are higher than 0.21  $\text{dpm cm}^{-2}$ , the cumulative standing stock of  $^{239,240}\text{Pu}$  expected from direct atmospheric fallout. Only beyond the shelf break at water depths deeper than 800 m are lower  $^{239,240}\text{Pu}$  inventories ( $< 0.21 \text{ dpm cm}^{-2}$ ) found. This reflects the fact that, compared with  $^{137}\text{Cs}$ , Pu has much higher affinity for particles and therefore can be more easily scavenged from the water column.

## Acknowledgements

The author wishes to thank Mr. Yong-Ching Huang for assisting in radiochemical analysis in the laboratory and to the crew of the R/V *Ocean Researcher-1* for assistance in sampling at sea. We appreciate the reviews by the editor and Drs. S.A. Kuehl and M. Baskaran. This work was supported by grants NSC86-2611-M-001-001-K2 and NSC87-2611-M-001-001-K2 from R.O.C National Science Council.

## References

- Aller, R.C., 1977. The influence of macrobenthos on chemical diagenesis of marine sediments. PhD Dissertation, Yale University, 600 pp.
- Appleby, P.G., Oldfield, F., 1992. Application of lead-210 to sedimentation studies. In: Ivanovich, M., Harmon, R.S. (Eds.), Uranium-series Disequilibrium—Applications to Earth, Marine, and Environmental Sciences. Oxford Science Publications, pp. 731–778.
- Chen, S.K., 1995. Sediment accumulation rates and organic carbon deposition in the East China Sea continental margin sediments. MS Thesis, National Taiwan University, Taipei, Taiwan, 80 pp.
- Chung, Y., Chang, W.C., 1995. Pb-210 fluxes and sedimentation rates on the lower continental slope between Taiwan and the South Okinawa Trough. *Continental Shelf Research* 15, 149–164.
- Comans, R.N.J., Middelburg, J.J., Zonderhuis, J., Woittiez, J.R.W., De Lange, G.J., Das, H.A., Van Der Weijden, C.H., 1989. Mobilization of radicaesium in pore water of lake sediments. *Nature* 339, 367–369.
- DeMaster, D.J., McKee, B.A., Nittrouer, C.A., Qian, J., Cheng, G., 1985. Rates of sediment accumulation and particle reworking based on radiochemical measurements from continental shelf deposits in the East China Sea. *Continental Shelf Research* 4, 143–158.
- Guinasso, N.L., Schink, D.R., 1975. Quantitative estimate of biological mixing rates in abyssal sediments. *J. Geophys. Res.* 80, 3032–3043.
- Hardy, E.P., Krey, P.W., Volchok, H.L., 1973. Global inventory and distribution of fallout plutonium. *Nature* 241, 444–445.
- Huang, Y., Shi, W., Chen, W., Li, K., Xie, J., 1983. Determination of sedimentation rates of continental shelf in the East China Sea using  $^{210}\text{Pb}$  dating technique. In: *Sedimentation on the Continental Shelf, with Special Reference to the East China Sea*. China Ocean Press, pp. 580–589.
- Huh, C.-A., Chen, H.-Y., 1999. History of lead pollution recorded in East China Sea sediments. *Marine Pollution Bulletin*, in press.
- Huh, C.-A., Zahnle, D.L., Small, L.F., Noshkin, V.E., 1987. Budgets and behaviors of uranium and thorium series isotopes in Santa Monica Basin sediments. *Geochim. Cosmochim. Acta* 51, 1743–1754.
- Huh, C.-A., Small, L.F., Niemi, S., Finney, B.P., Hickey, B.M., Gorsline, D.S., Williams, P.M., 1990. Sedimentation dynamics in the Santa Monica–San Pedro Basin off Los Angeles: radiochemical, sediment trap and transmissometer studies. *Continental Shelf Research* 10, 137–164.
- Huh, C.-A., Chu, K.-S., Wei, C.-L., Liew, P.-M., 1996. Lead-210 and plutonium fallout in Taiwan as recorded at a subalpine lake. *Journal of Southeast Asian Earth Science* 14, 373–376.
- Kempe, S., 1995. Coastal seas: a net source or sink of atmospheric carbon dioxide? LOICZ Reports and Studies No. 1. LOICZ, Texel, the Netherlands, 27 pp.
- Lee, H.J., Chough, S.K., 1989. Sediment distribution, dispersal and budget in the Yellow Sea. *Marine Geology* 87, 192–205.

- Li, Y.H., 1976. Denudation of Taiwan Island since the Pliocene Epoch. *Geology* 4, 105–107.
- Miller, K.M., Heit, M., 1986. A time resolution methodology for assessing the quality of lake sediment cores that are dated by  $^{137}\text{Cs}$ . *Limnol. Oceanogr.* 31, 1292–1300.
- Milliman, J.D., Meade, R.H., 1983. World-wide delivery of river sediment to the oceans. *Journal of Geology* 91, 1–21.
- Milliman, J.D., Qin, Y., Park, Y.A., 1989. Sediments and sedimentary processes in the Yellow and East China Seas. In: Taira, A., Masuda, A. (Eds.), *Sedimentary Facies in the Active Plate Margin*, pp. 233–249.
- Narita, H., Harada, K., Tsunogai, S., 1990. Lateral transport of sediment particles in the Okinawa Trough determined by natural radionuclides. *Geochemical Journal* 24, 207–216.
- Nozaki, Y., Tsunogai, S., 1973. Lead-210 in the north Pacific and the transport of terrestrial material through the atmosphere. *Earth Planet. Sci. Lett.* 20, 88–92.
- Ruddiman, W.F., Glover, L.K., 1972. Vertical mixing of ice-rafted volcanic ash in North Atlantic sediments. *Bull. Geol. Soc. Am.* 83, 2817–2836.
- Sholkovitz, E.R., 1983. The geochemistry of plutonium in fresh and marine water environments. *Earth-Science Reviews* 19, 95–161.
- Su, X., Zhou, H., Zeng, W., 1983. The recent sedimentation rates and processes in the Changjiang Estuary and its adjacent continental shelf area. In: *Sedimentation on the Continental Shelf, with Special Reference to the East China Sea*. China Ocean Press, pp. 562–571.
- Tsunogai, S., Shinagawa, T., Kurata, T., 1985. Deposition of anthropogenic sulfate and Pb-210 of the western North Pacific area. *Geochemical Journal* 19, 77–90.
- Turekian, K.K., Cochran, J.K., DeMaster, D.J., 1978. Bioturbation in deep-sea deposits: rates and consequences. *Oceanus* 21, 34–41.
- United Nations Scientific Committee on the Effects of Atomic Radiation (UNSCEAR), 1982. *Ionizing Radiation: Sources and Biological Effects*. Report to the General Assembly, with Annexes, 773 pp.
- Water Resources Planning Commission, 1996. *Hydrological Year Book of Taiwan, R.O.C., 1994*. Ministry of Economic Affairs.
- Yanagi, T., Morimoto, A., Ichikawa, K., 1997. Seasonal variation in surface circulation of the East China Sea and the Yellow Sea derived from satellite altimetric data. *Continental Shelf Research* 17, 655–664.
- Yeh, J.-C., Chung, Y.-C., 1997.  $^{228}\text{Ra}$  and  $^{226}\text{Ra}$  distributions off north and southwest Taiwan. *Terrestrial, Atmospheric and Oceanic Sciences* 8, 141–154.
- Zhang, J., 1996. Nutrient elements in the Chinese estuaries. *Continental Shelf Research* 16, 1023–1045.